REPORT SD-TR-89-73

Minimization of Intermodulation in GaAs MESFET Small-Signal Amplifiers

A. M. CROSMUN and S. A. MAAS
Electronics Research Laboratory
Laboratory Operations
The Aerospace Corporation
El Segundo, CA 90245

30 September 1989

Prepared for

SPACE SYSTEMS DIVISION
AIR FORCE SYSTEMS COMMAND
Los Angeles Air Force Base
P.O. Box 92960
Los Angeles, CA 90009-2960

This report was submitted by The Aerospace Corporation, El Segundo, CA 90245, under Contract No. F04701-85-C-0086-P00019 with the Space Systems Division, P.O. Box 92960, Los Angeles, CA 90009-2960. It was reviewed and approved for The Aerospace Corporation by M. J. Daugherty, Director, Electronics Research Laboratory.

Lt Boyle was the project officer for the Mission-Oriented Investigation and Experimentation (MOIE) Program.

This technical report has been reviewed and is approved for publication. Publication of this report does not constitute Air Force approval of the report's findings or conclusions. It is published only for the exchange and stimulation of ideas.

Steven L. Boyle

STEVE BOYLE, LT, USAF
MOIE Project Officer
SSD/CWHB

Raymond M Leong

RAYMOND M. LEONG, MAJ, USAF
MOIE Program Manager
AFSTC/WCO OL-AB

UNCLASSIFIED

SECURITY CLASSIFICATION OF THIS PAGE

REPORT DOCUMENTATION PAGE

1a. REPORT SECURITY CLASSIFICATION Unclassified	1b. RESTRICTIVE MARKINGS
2a. SECURITY CLASSIFICATION AUTHORITY	3. DISTRIBUTION/AVAILABILITY OF REPORT Approved for public release; distribution unlimited.
2b. DECLASSIFICATION/DOWNGRADING SCHEDULE	
4. PERFORMING ORGANIZATION REPORT NUMBER(S) TR-0089(4925-02)-4	5. MONITORING ORGANIZATION REPORT NUMBER(S) SD-TR-89-73
6a. NAME OF PERFORMING ORGANIZATION The Aerospace Corporation Laboratory Operations 6b. OFFICE SYMBOL *(If applicable)*	7a. NAME OF MONITORING ORGANIZATION Space Systems Division
6c. ADDRESS *(City, State, and ZIP Code)* El Segundo, CA 90245-4691	7b. ADDRESS *(City, State, and ZIP Code)* Los Angeles Air Force Base Los Angeles, CA 90009-2960
8a. NAME OF FUNDING/SPONSORING ORGANIZATION 8b. OFFICE SYMBOL *(If applicable)*	9. PROCUREMENT INSTRUMENT IDENTIFICATION NUMBER F04701-88-C-0089
8c. ADDRESS *(City, State, and ZIP Code)*	10. SOURCE OF FUNDING NUMBERS PROGRAM ELEMENT NO. / PROJECT NO. / TASK NO. / WORK UNIT ACCESSION NO.

11. TITLE *(Include Security Classification)*

Minimization of Intermodulation in GaAs MESFET Small-Signal Amplifiers

12. PERSONAL AUTHOR(S)

Crosmun, Andrea M.; Maas, Stephen A.

13a. TYPE OF REPORT	13b. TIME COVERED	14. DATE OF REPORT *(Year, Month, Day)*	15. PAGE COUNT
	FROM _____ TO _____	1989 September 30	30

16. SUPPLEMENTARY NOTATION

17. COSATI CODES		
FIELD	GROUP	SUB-GROUP

18. SUBJECT TERMS *(Continue on reverse if necessary and identify by block number)*

FET amplifiers
Intermodulation distortion
Nonlinear distortion
Volterra series

19. ABSTRACT *(Continue on reverse if necessary and identify by block number)*

This report examines the dependence of third-order intermodulation distortion on the source reflection coefficient Γ_s as a function of frequency, in an amplifier designed according to available-gain criteria. By means of a numerical formulation of the Volterra series, a complete equivalent circuit of the FET can be used, and intermodulation calculations include all feedback effects. We show that the sensitivity of IP_3 to Γ_s decreases with increasing frequency and can be related to the MESFET's stability.

20. DISTRIBUTION/AVAILABILITY OF ABSTRACT	21. ABSTRACT SECURITY CLASSIFICATION
☒ UNCLASSIFIED/UNLIMITED ☐ SAME AS RPT. ☐ DTIC USERS	Unclassified
22a. NAME OF RESPONSIBLE INDIVIDUAL	22b. TELEPHONE *(Include Area Code)* / 22c. OFFICE SYMBOL

DD FORM 1473, 84 MAR

83 APR edition may be used until exhausted.
All other editions are obsolete

SECURITY CLASSIFICATION OF THIS PAGE

UNCLASSIFIED

PREFACE

The authors thank G. Stout and W. Yamada for assisting with the S-parameter measurements, R. Gowin for assisting with the fabrication of the test fixtures, W. Garber for making some of the dc device measurements, and M. Meyer for reviewing the manuscript.

CONTENTS

FIGURES

I. INTRODUCTION

Microwave GaAs MESFET devices are used as amplifiers in a variety of linear applications. However, when two or more signals are applied to a MESFET simultaneously, the nonlinear properties of this device can result in intermodulation (IM) distortion. This distortion has important effects on system performance, particularly in broadband communication systems. Thus, the minimization of IM distortion in GaAs MESFETs is often a critical requirement.

In this report we show how the IM performance of a small-signal amplifier can be optimized when the amplifier is designed according to available-gain criteria. In this process, the MESFET's output is conjugate-matched and its input is mismatched to obtain a specified value of gain. We choose this method because it generally results in better dynamic range than other options; these options are (1) matching the input and mismatching the output, or (2) simultaneously matching both the input and output (which is, in many cases, impossible). In available-gain design the value of source impedance that provides the desired gain is not unique, and can be selected to optimize IM levels.

In many cases the IM intercept point[1] is a valid figure of merit for IM performance. To obtain the intercept point one must first be able to predict third-order intermodulation products, which result from the nonlinearities in the circuit. In the past, several attempts have been made to model nonlinearities in GaAs FETs by using the harmonic-balance technique[2-4] or specialized, approximate techniques.[5] The Volterra series has also been used to model nonlinear distortion in MESFETs;[6-9] however, much of this work employs simplifying assumptions that inevitably reduce accuracy. For example, in the work by Gupta et al.[6] the second-degree terms in the Volterra-series expansions were set to zero. However, these second-order products have an effect on the third-order products and therefore must be taken into account. Minasian[7] and Lambrianou et al.[8] employ simplified, unilateral equivalent circuits of the MESFET.

These simplifying assumptions are employed to ease the painfully difficult task of generating Volterra kernels in algebraic form. In this work, however, we circumvent such limitations by calculating the kernels numerically; thus, no such simplifying assumptions are necessary, and we can use a complete equivalent circuit of the MESFET. Furthermore, we include the effects of all of the MESFET's feedback elements; these effects have not been examined previously. Because Volterra-series analysis operates entirely in the frequency domain, is noniterative, and requires no convergence process, it is highly efficient and thus is a practical technique for circuit optimization.[10]

II. MODELING THE MESFET

This work is based on the packaged Avantek AT10650-5 MESFET, a 0.5 × 250-μm device that is similar in structure and performance to many commercial Ku-band MESFETs. The MESFET chip and its package are modeled by a lumped-element equivalent circuit, in which some of the elements are nonlinear. The modeling is performed in two steps: first, the equivalent circuit's linear elements are determined, then the characteristics of the nonlinear elements are measured. The dependence of the nonlinear elements on voltage are expressed via Taylor-series expansions of their current/voltage (I/V) or charge/voltage (Q/V) characteristics in the vicinity of their bias points.

The FETs used in this work were taken from a common fabrication lot. S-parameter data were measured from 45 MHz to 17 GHz, and several FETs having nearly identical S parameters and I/V characteristics were selected. The high-frequency data covering the range from 2 to 17 GHz were measured with the transistor biased at a drain voltage of 3.0 V and a drain current of 20 mA. The low-frequency S parameters were used primarily to model the drain-to-source conductance G_{ds}; therefore, these were obtained at several bias points near this operating point.

The equivalent-circuit elements were derived from a combination of dc and rf S-parameter measurements. Low-frequency Y parameters were used to obtain initial values for some of the elements, and the transconductance was derived from dc measurements. The resistances of the source and drain ohmic contacts were also derived from dc measurements by means of a method similar to that of Yang and Long[11] and modified by Fukai et al.[12] The small-signal linear circuit was then optimized to fit the measured high-frequency S parameters. When an adequate fit to the S parameters was obtained, techniques to model the nonlinear elements were employed. The complete model was simply a superposition of the nonlinear elements onto the linear model. The final circuit topology chosen to model the packaged

device is shown in Fig. 1, and the measured S parameters are compared in Fig. 2 to those of the model.

Modeling the nonlinear transconductance and drain-to-source resistance involves some subtleties. These two elements are derived from a single nonlinear drain-current source, $I_d(V_g,V_d)$, that is controlled by two voltages. In the small-signal case, this current source must be represented by a two-dimensional Taylor series. The small-signal incremental drain current $i_d(v_g,v_d)$ is

$$\begin{aligned} i_d(v_g,v_d) &= I_d(V_g,V_d) - I_d(V_{g0},V_{d0}) \\ &= \frac{\partial I_d}{\partial V_g} v_g + \frac{\partial I_d}{\partial V_d} + \frac{1}{2}\left[\frac{\partial^2 I_d}{\partial V_g^2} v_g^2 + 2\frac{\partial^2 I_d}{\partial V_g \partial V_d} v_g v_d + \frac{\partial^2 I_d}{\partial V_d^2} v_d^2\right] \\ &+ \frac{1}{6}\left[\frac{\partial^3 I_d}{\partial V_g^3} v_g^3 + 3\frac{\partial^3 I_d}{\partial V_g \partial V_d^2} v_g v_d^2 + 3\frac{\partial^3 I_d}{\partial V_g^2 \partial V_d} v_g^2 v_d + \frac{\partial^3 I_d}{\partial V_d^3} v_d^3\right] + \cdots \end{aligned} \tag{1}$$

where V_{g0} and V_{d0} are the bias voltages and v_g and v_d are the incremental gate and drain voltages, respectively, as shown in Fig. 3. In the linear equivalent circuit, the drain current is expressed by the linear terms in Eq. (1); thus

$$i_d(v_g,v_d) = \frac{\partial I_d}{\partial V_g} v_g + \frac{\partial I_d}{\partial V_d} v_d \tag{2}$$

or

$$i_d(v_g,v_d) = g_m(V_{g0},V_{d0})v_g + G_{ds}(V_{g0},V_{d0})v_g \tag{3}$$

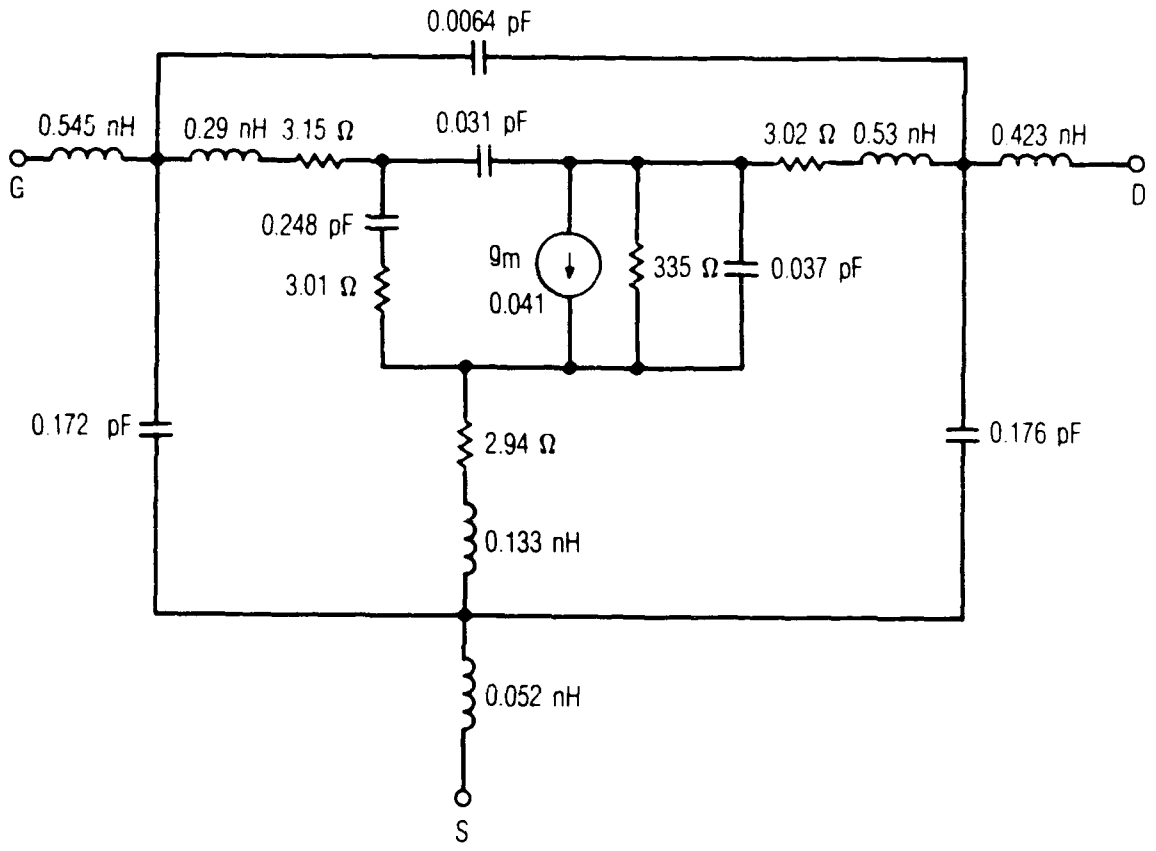

Fig. 1. Linear Lumped Equivalent-Circuit Model of the Packaged AT10650-5 MESFET

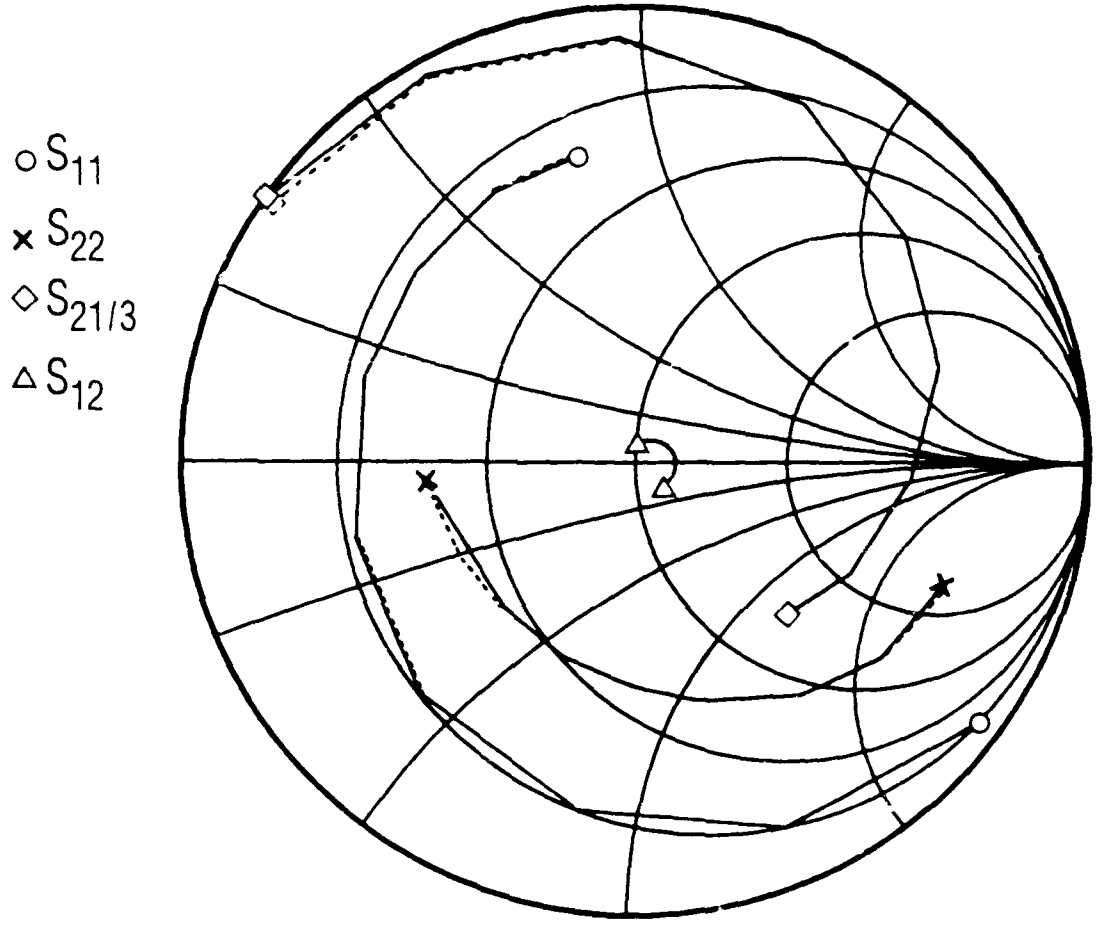

Fig. 2. Measured S Parameters of the AT10650-5 MESFET at a 3-V, 20-mA Bias over the 2 to 14-GHz Range. The solid line represents measured data; the dotted line shows the S parameters calculated from the model in Fig. 1.

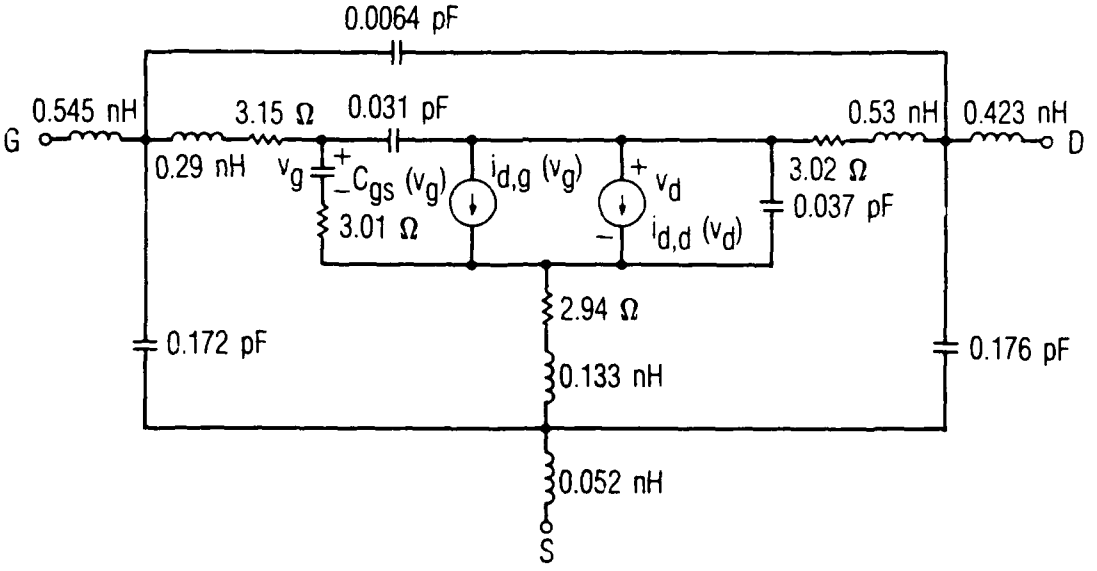

Fig. 3. Nonlinear Equivalent Circuit of the MESFET in the Vicinity of the 3-V, 20-mA Bias Point. $i_{d,g}$ coefficients are $a_1 = 0.041$, $a_2 = 0.0171$, $a_3 = -0.0145$; $i_{d,d}$ coefficients are $b_1 = 0.0030$, $b_2 = 3.09 \times 10^{-4}$, $b_3 = 3.99 \times 10^{-5}$; $V_{g0} = 0.54$ V.

and the small-signal drain current can be modeled by means of a pair of separate elements, the controlled source g_m and the controlled conductance G_{ds}.

In the nonlinear case the controlled source and conductance are traditionally modeled as two separate nonlinear elements, each controlled by a single voltage; thus

$$i_d(v_g,v_d) = i_{d,g}(v_g) + i_{d,d}(v_d) \tag{4}$$

where

$$i_{d,g}(v_g) = a_1v_g + a_2v_g^2 + a_3v_g^3 \tag{5}$$

and

$$i_{d,d}(v_d) = b_1v_d + b_2v_d^2 + b_3v_d^3 \tag{6}$$

The a_n and b_n coefficents are the $\partial^n I_d/\partial V_g^n$ and $\partial^n I_d/\partial V_d^n$ terms in Eq. (1); from Eqs. (1) through (3), $a_1 = g_m$ and $b_1 = G_{ds}$. Although it is clear that the cross terms are usually much smaller than the terms involving V_g, they are sometimes not small compared to those involving V_d. The terms involving V_d are rarely dominant, but they may still be significant; thus, these cross terms may also be significant.

The modeling of $i_{d,g}$ is further complicated by its weak nonlinearity, especially near the bias points that would normally be used for high-dynamic-range amplifiers. Because this nonlinearity is so weak, even small uncertainties in measurement and low levels of quantization noise may obscure the curvature in $i_{d,g}$. Even when the noise level is low, the direct differentiation of $i_{d,g}$ to obtain the derivatives in Eq. (1) increases the noise level and makes unreliable the derivatives beyond the second. Furthermore, least-square fitting to a polynomial, a commonly used alternative, often fails because the ill-conditioned nature of the normal

equation makes the process overly sensitive to small changes in the measured I/V data.

Another problem is the well-known frequency dependence of G_{ds}, which is often attributed to traps in the MESFET's channel. These traps cause the value of G_{ds} measured above 1 MHz to be one-fifth to one-half the dc value, and they have effects on the higher derivatives $\partial I_d^n / \partial V_d^n$ that are difficult to characterize.

Because of these effects, it is usually not possible to determine the derivatives in Eq. (1) by dc measurements. The cross terms are even more difficult to measure than the others, so there is little choice but to neglect them and to model $i_d(v_g, v_d)$ as two separate, singly controlled nonlinear elements. The consequences of this approach are acceptable in circuits in which $i_{d,g}(v_g)$ is the dominant nonlinearity; this is the case in virtually all modern MESFETs.

These considerations are not unique to Volterra-series analysis. They apply to any form of analysis used to calculate small-signal nonlinear effects in FET amplifiers, particularly harmonic-balance analysis. Because harmonic-balance analysis is applied primarily to large-signal circuits, the models are usually designed to describe the MESFET over the entire range of drain-to-source and gate-to-source voltages. However, these models may not accurately express the derivatives in Eq. (1) in the vicinity of a specific bias point, and their use may result in incorrect results when applied to small-signal distortion problems.

The a_n terms in Eq. (5), which represent a nonlinear controlled current source, were determined by the method described in Ref. 13. This method involves extracting the source's Taylor-series coefficients from harmonic measurements at low frequencies. The b_n terms in Eq. (6) represent a nonlinear conductance. These were found by numerically differentiating values of G_{ds} obtained from low-frequency Y parameters over a range of values of v_d; because the curvature of $G_{ds}(V_d)$ was much greater than the uncertainties in the data, and only two derivatives need be taken, a

multipoint derivative formula gave good results. Because it is based partly on dc measurements, this process only partially compensates for the frequency sensitivity of G_{ds}.

The value of gate capacitance C_{gs} varies with V_g, the voltage across the capacitor's terminals. C_{gs} behaves as a uniformly doped Schottky-barrier diode capacitance having the controlling voltage v_g, and was modeled as such. The nonlinear MESFET model was established by including the nonlinearity of C_{gs}, G_{ds}, and g_m in the linear equivalent circuit of Fig. 1. The nonlinear equivalent circuit is shown in Fig. 3.

III. CALCULATIONS

The available gain of a two-port is a function solely of the source reflection coefficient Γ_s; the locus of Γ_s values that provide a specific value of gain lie on a circle in the Γ_s plane. The available-gain and stability circles of the GaAs FET were plotted on a Smith chart for three cases: 2, 5, and 10 GHz. Intermodulation (IM) products were calculated at points chosen periodically along the gain circles to find values that would maximize the amplifier's third-order intercept point, IP_3. The stability circles and the corresponding intercept points are shown in Figs. 4, 5, and 6.

In order to calculate the IP_3 values, it was necessary to modify the FET model to account for differences between the coaxial transistor test fixture (TTF) and microstrip amplifier environments. The TTF measurements included the inductance of a short section of gate and drain leads, and these excess lengths do not exist in the amplifier. The model was therefore modified by the removal of these added inductances, and the data shown in Figs. 4 through 6 do not include them.

The process of calculating the intercept points is implemented numerically, and thus is straightforward. In practice, it is necessary only to create a data file that describes the circuit elements and their nodal interconnections, along with ancillary information such as frequencies and the mixing product of interest (the appearance of the data file is similar to that of nodal-entry linear circuit-analysis programs.) The element catalog includes both lumped and distributed elements, including a microstrip model that accounts for loss and dispersion. It is necessary, in the case of nonlinear elements, to include the Taylor-series coefficients, although the program can generate them for elements having well-established nonlinear characteristics (e.g. diode-junction conductance and capacitance). Arbitrary source- or load-impedance data are entered via a disk file. The program requires only a few seconds per data point when run on an 8-MHz IBM PC-AT desktop computer.

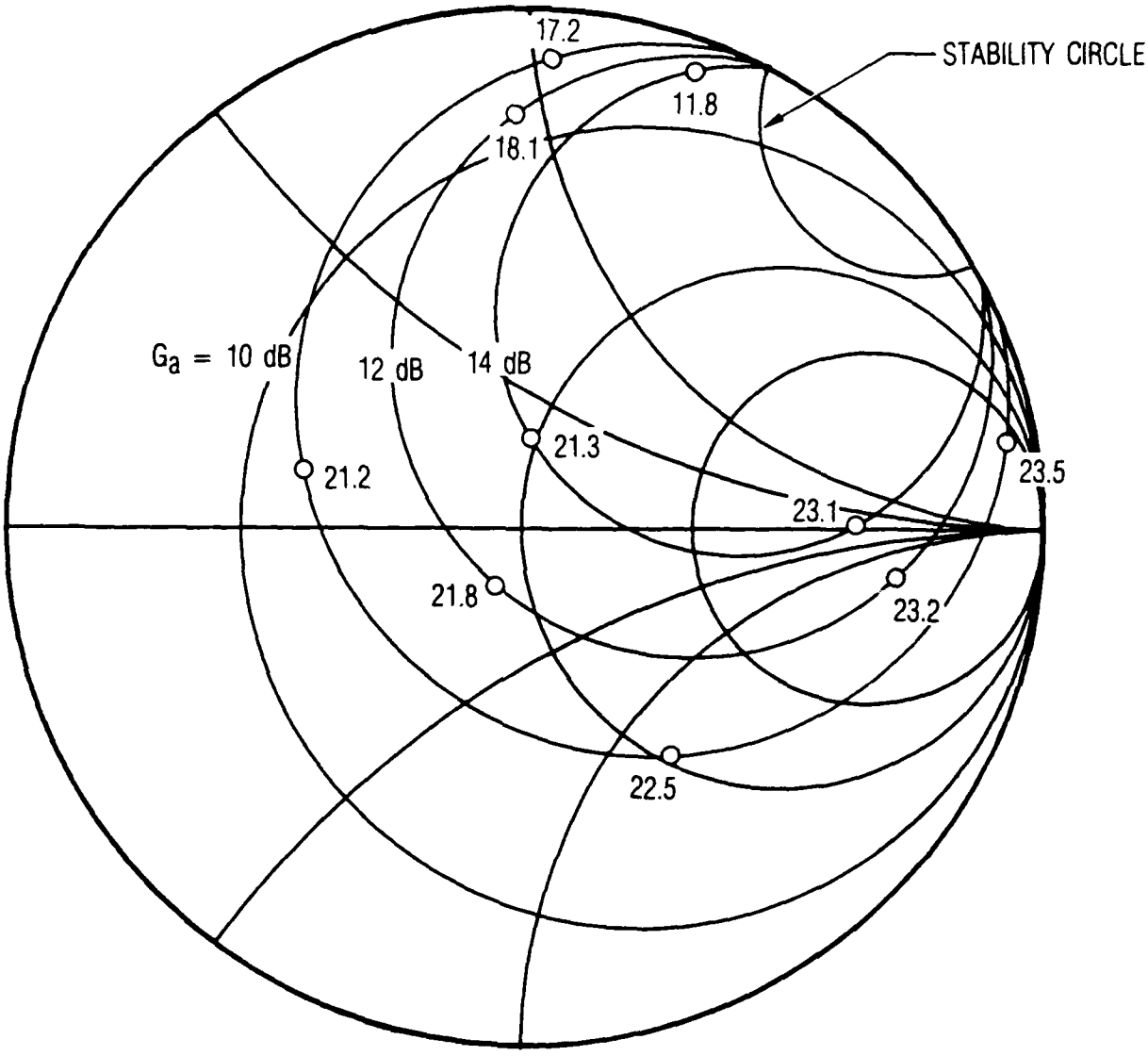

Fig. 4. Gain and Stability Circles and Calculated Third-Order Intercept Points of the MESFET at 2 GHz

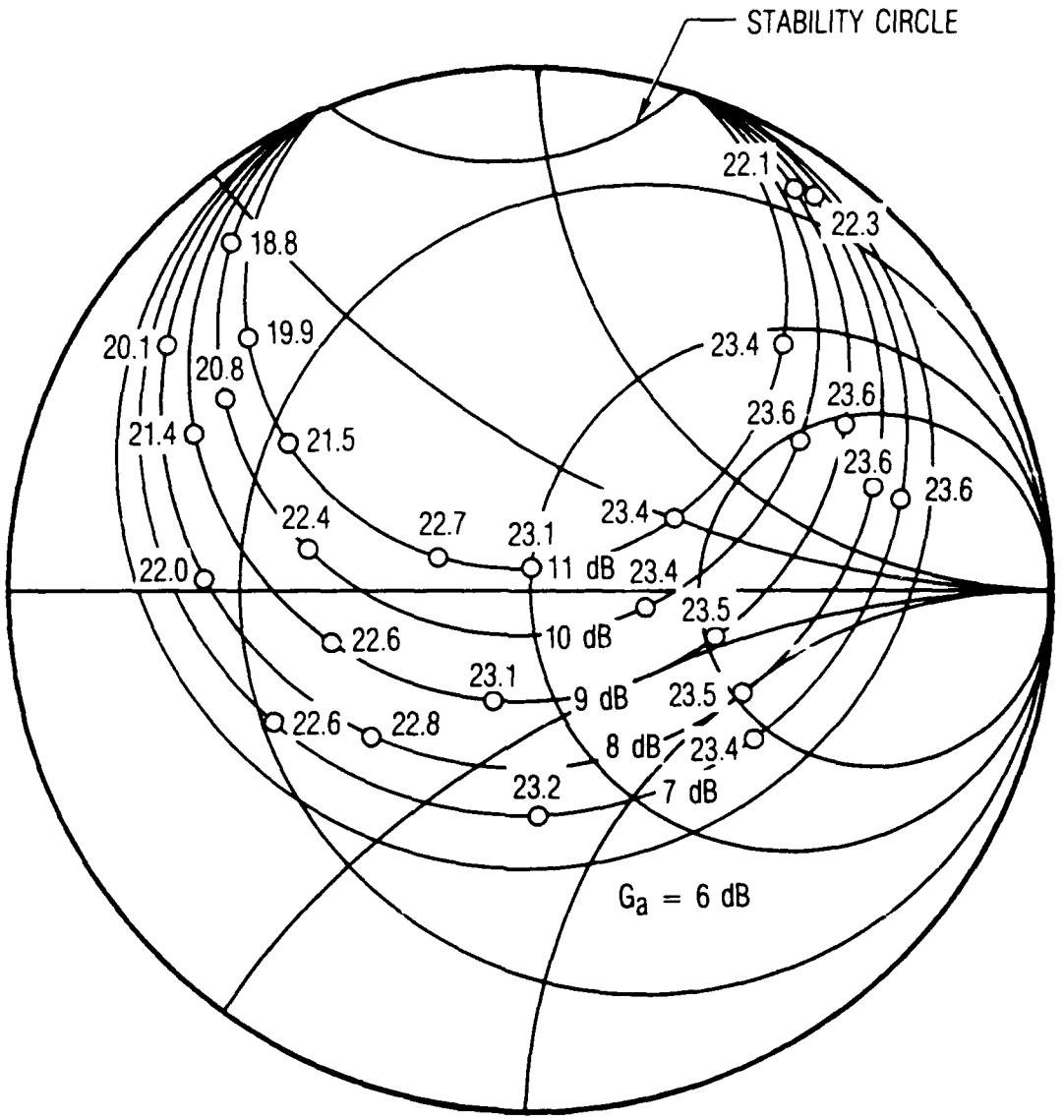

Fig. 5. Gain and Stability Circles and Calculated Third-Order Intercept Points of the MESFET at 5 GHz

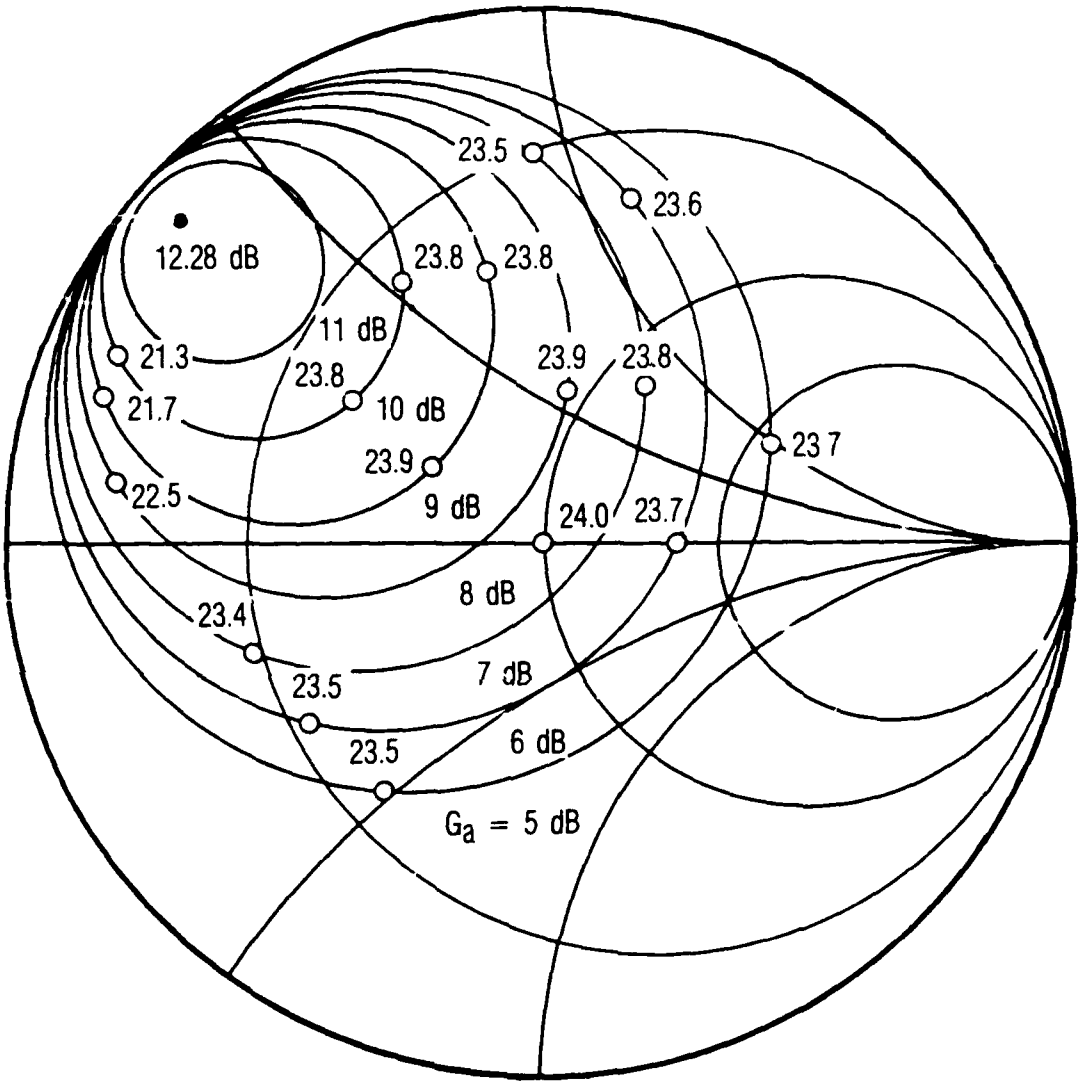

Fig. 6. Gain and Stability Circles and Calculated Third-Order Intercept Points of the MESFET at 10 GHz

The program is based on an implementation of the Volterra series called the method of nonlinear currents.[1] This method converts the weakly nonlinear circuit into a linear circuit and a set of current sources whose currents are, at each order, a function of all lower-order node voltages. The program operates by first determining the linear, or first-order, voltages at each of the circuit's nodes. It then uses these voltages to generate excitation-current sources at the second-order mixing frequencies; each nonlinear element is replaced by one such source. The remainder of the circuit is linear, and can be solved to obtain second-order voltages by conventional nodal methods. Similarly, the third-order mixing products are found from the first- and second-order products. The method includes the effect of all lower-order mixing products on each higher-order mixing product.

IV. RESULTS

The intercept points calculated for the 10- and 5-GHz amplifier gain circles were verified experimentally by measuring the IM levels of several amplifiers designed for these frequencies. Because the IM levels were relatively independent of Γ_s at 10 GHz, only the point $\Gamma_s = 0$ was tested, with the load reflection coefficient Γ_L equal to zero and a conjugate match. For the 5-GHz case, however, several configurations were built and tested in an attempt to cover the range of values of Γ_s that displayed significant variation in IM level.

For the first 10-GHz case an amplifier was built with Γ_s, $\Gamma_L = 0$. The measured gain of this amplifier was 4.5 dB, and the intercept point was found to be 22.4 dBm. The calculated values were 5.0 dB and 20.9 dBm, respectively. With the output conjugately matched, the gain improved to 6.8 dB and the output intercept point was 23.5 dBm. Calculated values under these conditions were 6.1 dB and 24.1 dBm, respectively.

To verify the 5-GHz theoretical results, several points in the Γ_s plane were tested experimentally. These tests required an amplifier whose input matching circuit could present a range of Γ_s values (from the worst to the optimum intercept-point locations) on various gain circles. This input circuit consisted of a quarter-wave transformer and a length of 50-ohm line. Γ_s was varied by trimming the width of the microstrip transformer; thus its impedance increased each time it was cut. The output was conjugate matched in each case by means of a tuner, and intercept points were measured via a two-tone test. In this way, the intercept points for eight Γ_s values were obtained.

The transformer's step-discontinuity reactances are an important component of Γ_s. Unfortunately, attempts to model these reactances via closed-form quasistatic approximations were not successful, because of the limited accuracy of such formulations. To determine these values, we note that the dominant effect of the transformer is to change the magnitude

of Γ_s, while the discontinuities primarily affect the phase. Thus, one can find $|\Gamma_s|$ from the transformer impedance, and $\angle \Gamma_s$ as the point where the $|\Gamma_s|$ curve intersects the gain circle. This heuristic approach treats the FET's measured S parameters as a standard. This is reasonable, because the FET's S parameters -- measured by an accurately calibrated automatic network analyzer -- are known more accurately than the discontinuity reactances.

The experimental intercept points and the calculated data are plotted on a Smith chart in Fig. 7; the gain and IP_3 values are corrected for the loss in the output tuner (0.7 dB). The difference between the calculated and measured IP_3 values in most cases is less than 1 dB.

At 10 GHz the MESFET is unconditionally stable. It is evident from Fig. 6 that the intercept points in this case do not vary much along the gain circles, or even from one gain circle to another; the distortion levels are already minimal for unconditionally stable conditions. This insensitivity of IP_3 to Γ_s is a characteristic of unilateral circuits.[1] We believe that the reason for the insensitivity of IP_3 to Γ_s is a manifestation of the fact that feedback effects are minimal in an unconditionally stable circuit. Thus, in terms of its IP_3 characteristics, the amplifier behaves much like a unilateral circuit.

At 5 GHz the MESFET is conditionally stable and has optimum values of Γ_s for minimizing third-order intermodulation distortion. Figure 5 shows that the intercept points are highest near the counter-clockwise extreme of the gain circles, and are nearly independent of gain. At the clockwise extreme, the intercepts are lower and are much more sensitive to gain; the IP_3 values increase as gain decreases. In general, the intercept points are lower in regions near the stability circle.

The same conclusions can be deduced from the 2-GHz case shown in Fig. 4, except that the effects are more pronounced. The best performance is obtained near the counter-clockwise end of the gain circle, and the worst performance -- a 12-dB reduction in IP_3 -- occurs near the clockwise end.

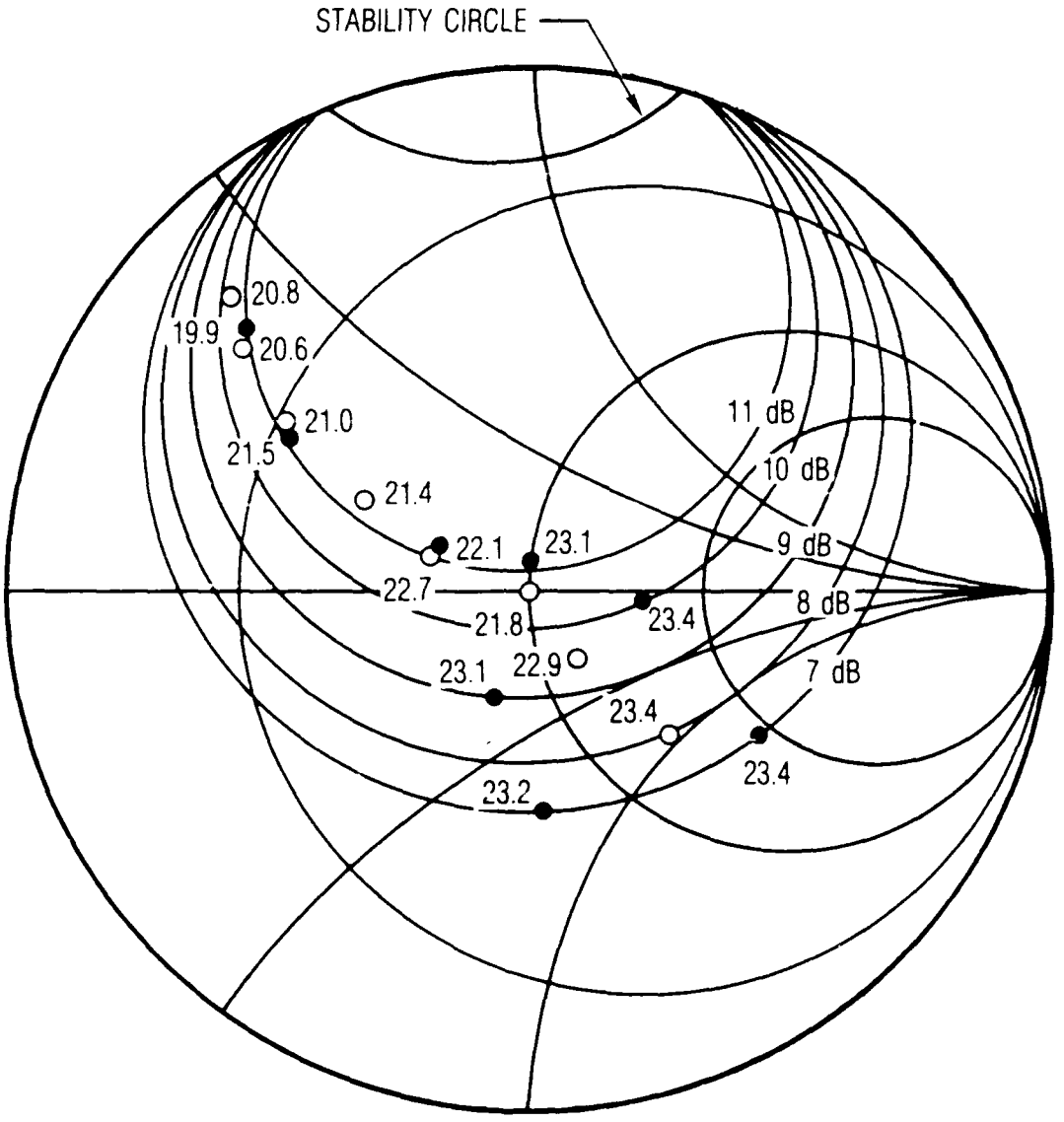

Fig. 7. Gain and Stability Circles and Third-Order Intercept Points of the MESFET at 5 GHz. Calculated IP_3 values are indicated by filled circles, measured values by open circles.

Figures 8 and 9 show the sensitivity of IP_3 to source and load impedance when no gain constraint is imposed. It is clear from these figures that the intrinsic sensitivity of IP_3 to load impedance is much greater than the sensitivity to source impedance (however, if IP_3 were defined in terms of available input power, a definition that sometimes is more relevant, the sensitivity to Γ_s would be greater). This sensitivity to load impedance is reflected in the data of the earlier figures: at 10 GHz, where the FET is unconditionally stable and thus feedback effects are minimal, the value of Γ_L that results in a conjugate match is close to $S_{2,2}^*$ and does not vary much as Γ_s is varied. Consequently, the IP_3 does not vary significantly with Γ_s. However, at 5 GHz the FET is conditionally stable and Γ_L varies more strongly with Γ_s; the sensitivity of Γ_L to Γ_s is especially severe at 2 GHz. It is interesting to note that the worst values of IP_3 are strongly associated with highly reactive values of Γ_L. These results are consistent with an experimental study of IM in MESFETs that identified $\Gamma_L \approx S_{2,2}^*$ as a good estimate of the load impedance that *maximized* IP_3.[14]

Fortunately, the values of Γ_s that optimize the intercept point are generally in the same region of the input plane as those that optimize the noise figure. Thus, at a given bias level the trade-off between noise and linearity in a FET amplifier may not be very severe. However, the bias conditions that optimize noise figure ($I_d \approx 0.15 I_{dss}$) and those that optimize IP_3 ($I_d \approx 0.50 I_{dss}$) present a substantial trade-off.

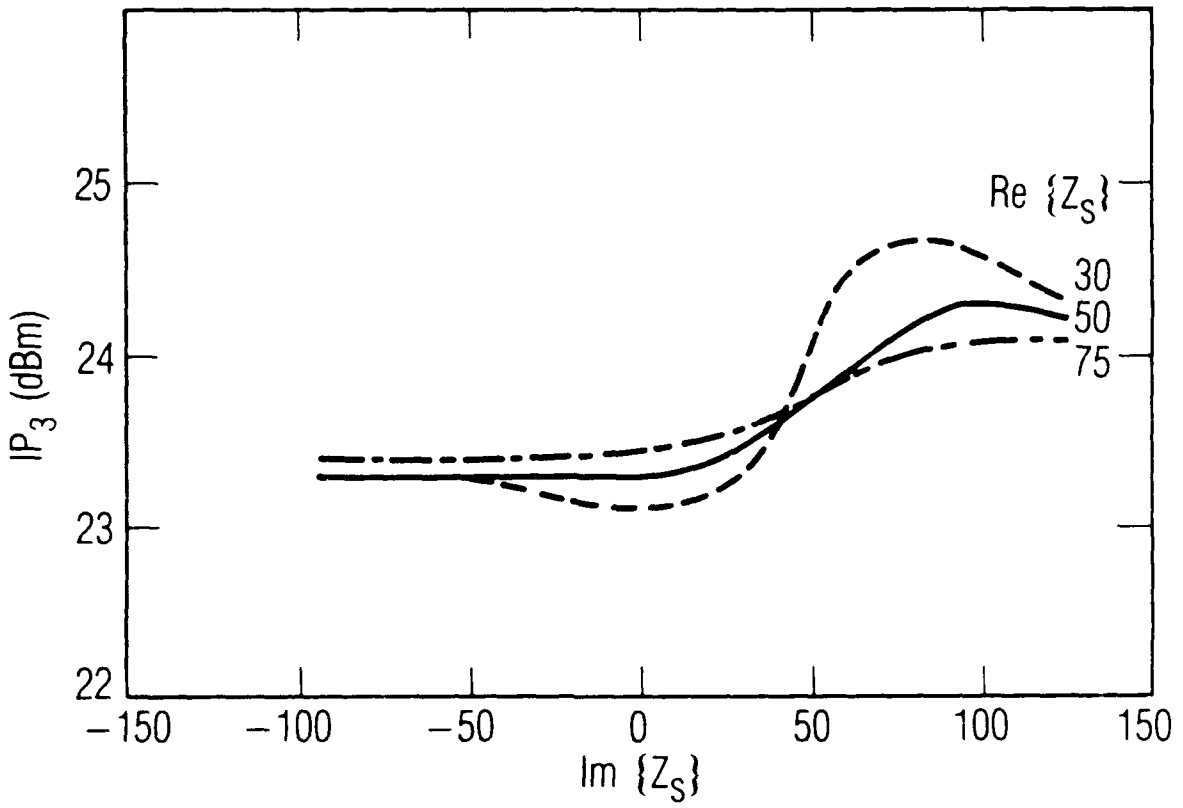

Fig. 8. Sensitivity of IP_3 to Z_S at 5 GHz. Z_L = j86 (this is the optimum value of Z_L when Z_S = 50 + j0).

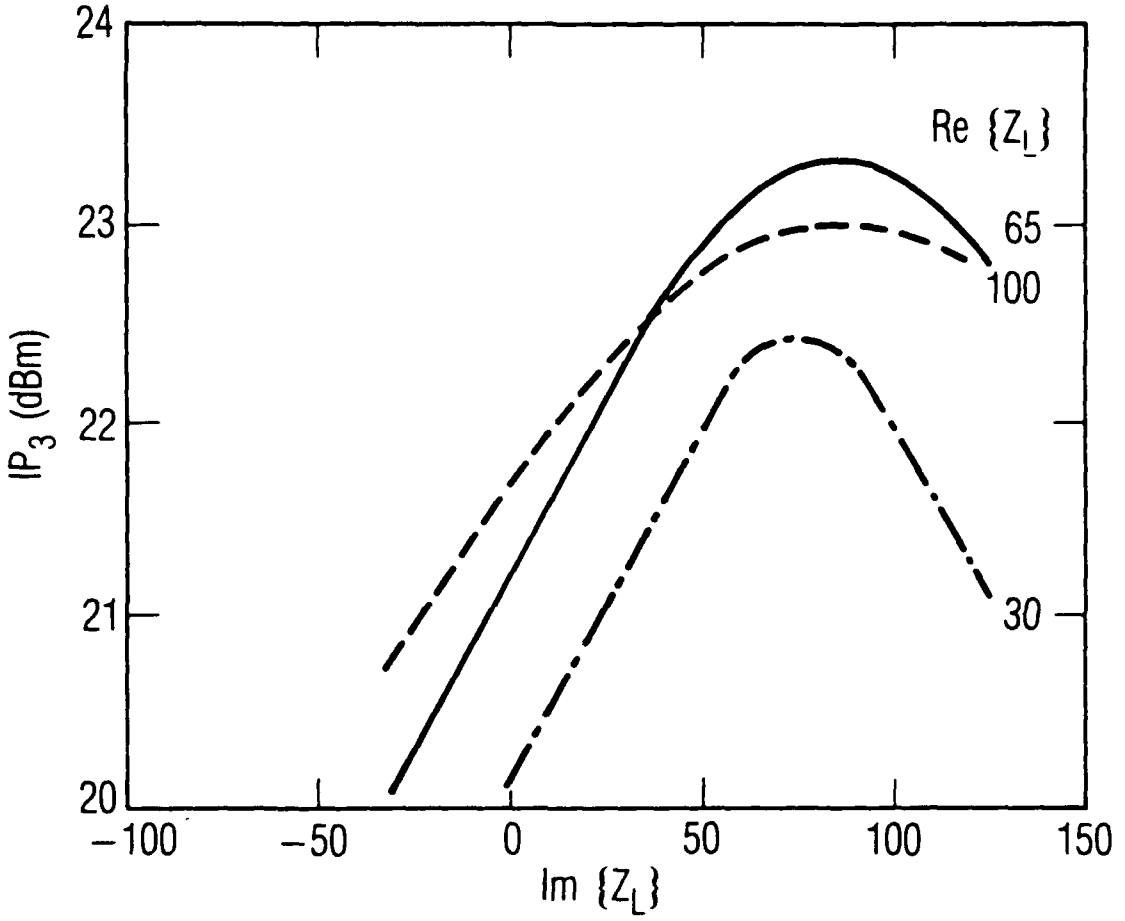

Fig. 9. Sensitivity of IP_3 to Z_L at 5 GHz. Z_s = 50 + j0.

V. CONCLUSIONS

These results show that this approach to optimizing intercept points is practical and accurate. The measured and predicted intercept points fall within approximately 1.5 dB of each other, which is little more than the uncertainty in the measurements themselves. The use of a complete MESFET model makes the results particularly meaningful, because no significant effects related to the circuit topology (e.g. feedback phenomena) are ignored.

Under available-gain constraints, the MESFET's output IP_3 is sensitive to Γ_s. At low frequencies, where the MESFET is conditionally stable, the MESFET's IP_3 is most sensitive to Γ_s. However, as frequency is increased, that sensitivity decreases and essentially disappears at the point where the MESFET becomes unconditionally stable. This sensitivity is the result of feedback effects that cause the conjugate-match Γ_L to be highly reactive. When gain constraints are removed, the sensitivity of output IP_3 to Γ_L is greater than its sensitivity to Γ_s.

Conventional methods of modeling the drain-current nonlinearity do not include potentially significant effects in the device. Further research is needed to develop more accurate modeling techniques.

REFERENCES

1. S. Maas, Nonlinear Microwave Circuits (Artech House, Norwood, Mass., 1988).

2. R. Gilmore, "Nonlinear Circuit Design Using the Modified Harmonic-Balance Algorithm," IEEE Trans. Microwave Theory Tech. MTT-34, 1294 (1986).

3. W. R. Curtice, "Nonlinear Analysis of GaAs MESFET Amplifiers, Mixers, and Distributed Amplifiers Using the Harmonic Balance Technique," IEEE Trans. Microwave Theory Tech. MTT-35, 441 (1987).

4. V. Rizzoli, C. Cachetti, and A. Lipparini, "A General-Purpose Program for the Analysis of Nonlinear Microwave Circuits under Periodic Excitation by Multidimensional Fourier Transform," Proc. 17th European Microwave Conf., 1987, p. 635.

5. R. S. Tucker, "Third-Order Intermodulation Distortion and Gain Compression in GaAs FETs," IEEE Trans. Microwave Theory Tech. MTT-27, 400 (1979).

6. R. K. Gupta, L. G. Englefield, and P. A. Goud, "Intermodulation Distortion in Microwave MESFET Amplifiers," IEEE MTT-S Int. Microwave Symp. Digest (1978), p. 405.

7. R. A. Minasian, "Intermodulation Distortion Analysis of MESFET Amplifiers Using the Volterra Series Representation," IEEE Trans. Microwave Theory Tech. MTT-28, 1 (1980).

8. G. M. Lambrianou and C. S. Aitchison, "Optimization of Third-Order Intermodulation Product and Output Power from an X-Band MESFET Amplifier using Volterra Series Analysis," IEEE Trans. Microwave Theory Tech. MTT-33, 1395 (1985).

9. A. M. Crosmun, "Use of Volterra Series Analysis for Optimizing the Intercept Point of GaAs MESFET Small-Signal Amplifiers," M. S. Thesis, University of California, Los Angeles, 1988.

10. S. A. Maas, "A General-Purpose Computer Program for the Volterra-Series Analysis of Nonlinear Microwave Circuits," IEEE MTT-S Int. Microwave Symp. Digest (1988), p. 311.

11. L. Yang and S. I. Long, "New Method to Measure the Source and Drain Resistance of the GaAs MESFET," IEEE Trans. Electron Devices EDL-7, 75 (1986).

12. A. Fukai et al., private communication, The Aerospace Corporation.

13. S. A. Maas and A. M. Crosmun, "Modeling the Gate I/V Characteristics of a GaAs MESFET for Volterra-Series Analysis," submitted to IEEE Trans. Microwave Theory Tech., 1988.

14. C. Y. Ho and D. Burgess, "Practical Design of 2-4 GHz Low Inter-Modulation Distortion GaAs FET Amplifiers with Flat Gain Response and Low Noise Figure," Microwave J. 26, 91 (February 1983).

LABORATORY OPERATIONS

The Aerospace Corporation functions as an "architect-engineer" for national security projects, specializing in advanced military space systems. Providing research support, the corporation's Laboratory Operations conducts experimental and theoretical investigations that focus on the application of scientific and technical advances to such systems. Vital to the success of these investigations is the technical staff's wide-ranging expertise and its ability to stay current with new developments. This expertise is enhanced by a research program aimed at dealing with the many problems associated with rapidly evolving space systems. Contributing their capabilities to the research effort are these individual laboratories:

Aerophysics Laboratory: Launch vehicle and reentry fluid mechanics, heat transfer and flight dynamics; chemical and electric propulsion, propellant chemistry, chemical dynamics, environmental chemistry, trace detection; spacecraft structural mechanics, contamination, thermal and structural control; high temperature thermomechanics, gas kinetics and radiation; cw and pulsed chemical and excimer laser development including chemical kinetics, spectroscopy, optical resonators, beam control, atmospheric propagation, laser effects and countermeasures.

Chemistry and Physics Laboratory: Atmospheric chemical reactions, atmospheric optics, light scattering, state-specific chemical reactions and radiative signatures of missile plumes, sensor out-of-field-of-view rejection, applied laser spectroscopy, laser chemistry, laser optoelectronics, solar cell physics, battery electrochemistry, space vacuum and radiation effects on materials, lubrication and surface phenomena, thermionic emission, photosensitive materials and detectors, atomic frequency standards, and environmental chemistry.

Computer Science Laboratory: Program verification, program translation, performance-sensitive system design, distributed architectures for spaceborne computers, fault-tolerant computer systems, artificial intelligence, microelectronics applications, communication protocols, and computer security.

Electronics Research Laboratory: Microelectronics, solid-state device physics, compound semiconductors, radiation hardening; electro-optics, quantum electronics, solid-state lasers, optical propagation and communications; microwave semiconductor devices, microwave/millimeter wave measurements, diagnostics and radiometry, microwave/millimeter wave thermionic devices; atomic time and frequency standards; antennas, rf systems, electromagnetic propagation phenomena, space communication systems.

Materials Sciences Laboratory: Development of new materials: metals, alloys, ceramics, polymers and their composites, and new forms of carbon; nondestructive evaluation, component failure analysis and reliability; fracture mechanics and stress corrosion; analysis and evaluation of materials at cryogenic and elevated temperatures as well as in space and enemy-induced environments.

Space Sciences Laboratory: Magnetospheric, auroral and cosmic ray physics, wave-particle interactions, magnetospheric plasma waves; atmospheric and ionospheric physics, density and composition of the upper atmosphere, remote sensing using atmospheric radiation; solar physics, infrared astronomy, infrared signature analysis; effects of solar activity, magnetic storms and nuclear explosions on the earth's atmosphere, ionosphere and magnetosphere; effects of electromagnetic and particulate radiations on space systems; space instrumentation.